Functionally Graded Cathodes for Solid Oxide Fuel Cells

Final Report

Reporting Period: 1 July 2005 to 30 March 2007
DOE Contract No.: DE-FC26-05NT42515
DOE Project Manager: Dr. Lane Wilson

Prepared by

Harry Abernathy and Meilin Liu

Center for Innovative Fuel Cell and Battery Technologies
School of Materials Science and Engineering
Georgia Institute of Technology
Atlanta, GA 30332-0245

Report Issued: March 2007

DISCLAIMER

This report was prepared as an account of work sponsored by an agency of the United States Government. Neither the United States Government nor any agency thereof, nor any of their employees, makes any warranty, express of implied, or assumes any legal liability or responsibility for the accuracy, completeness, or usefulness of any information, apparatus, product, or process disclosed, or represents that its use would not infringe privately owned rights. Reference herein to any specific commercial product, process, or service by trade name, trademark, manufacturer, or otherwise does not necessarily constitute or imply its endorsement, recommendation, or favoring by the United States Government or any agency thereof. The views and opinions of authors expressed herein do not necessarily state or reflect those of the United States Government or any agency thereof.

ABSTRACT

One primary suspected cause of long-term performance degradation of solid oxide fuels (SOFCs) is the accumulation of chromium (Cr) species at or near the cathode/electrolyte interface due to reactive Cr molecules originating from Cr-containing components (such as the interconnect) in fuel cell stacks. To date, considerable efforts have been devoted to the characterization of cathodes exposed to Cr sources; however, little progress has been made because a detailed understanding of the chemistry and electrochemistry relevant to the Cr-poisoning processes is still lacking. This project applied multiple characterization methods – including various Raman spectroscopic techniques and various electrochemical performance measurement techniques – to elucidate and quantify the effect of Cr-related electrochemical degradation at the cathode/electrolyte interface. Using Raman microspectroscopy the identity and location of Cr contaminants ($SrCrO_4$, $(Mn/Cr)_3O_4$ spinel) have been observed *in situ* on an LSM cathode. These Cr contaminants were shown to form chemically (in the absence of current flowing through the cell) at temperatures as low as 625ºC. While $SrCrO_4$ and $(Mn/Cr)_3O_4$ spinel must preferentially form on LSM, since the LSM supplies the Sr and Mn cations necessary for these compounds, LSM was also shown to be an active site for the deposition of Ag_2CrO_4 for samples that also contained silver. In contrast, Pt and YSZ do not appear to be active for formation of Cr-containing phases. The work presented here supports the theory that Cr contamination is predominantly chemically-driven and that in order to minimize the effect, cathode materials should be chosen that are free of cations/elements that could preferentially react with chromium, including silver, strontium, and manganese.

TABLE OF CONTENTS

DISCLAIMER 2
ABSTRACT 3
TABLE OF CONTENTS 4
LIST OF GRAPHICAL MATERIALS 5
INTRODUCTION 6
EXECUTIVE SUMMARY 8
EXPERIMENTAL 10
RESULTS AND DISCUSSION 12
CONCLUSIONS 17
FIGURES AND TABLES 18
REFERENCES 28

LIST OF GRAPHICAL MATERIALS

Figure 1. (a) Schematic and (b) photograph of *in situ* Raman spectroscopy system. 18
Figure 2. (a) LSM/GDC composite and (b) micropatterned LSM electrode samples used for *in situ* Raman measurements. For the composite sample micrograph, the outlined red regions are LSM. 19
Figure 3. Creation of SERS effect on cathode surface by (a) evaporating Au/Ag colloids on cathode surface, (b) sputtering nano-sized Au/Ag islands on cathode, and (b) co-depositing cathode material along with Ag nanoparticles. 20
Figure 4. Raman spectra of various chromium-containing phases compared with the Raman spectra of standard SOFC components 21
Figure 5. (a) Microscope image of Cr_2O_3 powder (the light phase) on an LSM substrate (the dark phase). (b) Raman map plotting the intensity of the Raman signal at 550 cm^{-1} as a function of position. The brighter the green, the greater the signal intensity. Each pixel represents 1 μm^2. 21
Figure 6. Raman spectra from the LSM-GDC composite surface before and after exposure to humidified air for 24 hours. The spectra were collected at 650ºC. 22
Figure 7. Raman spectra collected from the silver counterelectrode surface before and after exposure to Cr-containing air at 650ºC for 36 hours without polarization. Both spectra were measured at room temperature. 22
Figure 8. Raman spectra from red deposit on LSM-GDC composite sample and from Ag_2CrO_4 powder. 23
Figure 9. Optical micrographs of micropatterned LSM sample at 625ºC exposed to Cr-containing vapor for (a) 0, (b) 5, and (c) 21 days. The orange line denotes an LSM-YSZ interface. Figure 9(b) shows the contact point between the silver wire and an LSM electrode. 23
Figure 10. Raman spectra collected *in situ* from the micropatterned LSM sample after exposure to Cr vapor at 625ºC for three weeks. 24
Figure 11. Raman map of Ag_2CrO_4 on a patterned LSM electrode (on a YSZ substrate) after exposure The Raman spectra for the map were collected *ex situ* at room temperature. . 24
Figure 12. (a) Raman spectra from patterned LSM electrode at 625ºC before and after exposure to Cr-containing humidified oxygen. (b) Spectra (1) and (2) were collected *ex situ* from the sample after 48 hrs exposure to Cr vapor. 25
Figure 13. Raman map plotting the integrated intensity of the 885 cm^{-1} peak from $SrCrO_4$ on the micropatterned LSM on YSZ sample exposed to Cr vapor for 48 at 625ºC. The map was generated *ex situ* at room temperature. The red box in the micrograph indicates the map area. 25
Figure 14. (a) *In situ* Raman spectra from dense LSM pellet at 625ºC before and after exposure to Cr-containing humidified oxygen for 24 hrs. (b) Spectra (1) and (2) were collected room temperature from the same sample. 26
Figure 15. *In situ* Raman spectra from Pt-YSZ composite at 625ºC before and after exposure to Cr-containing Cr vapor for 120 hrs. 26
Figure 16. Raman spectra of a Cr_2O_3 film deposited on an LSM substrate using CCVD with and without Ag nanoparticles. 27
Figure 17. Images of a sharp tungsten AFM tip (a) before and (b) after coating with silver. . 27
Figure 18. SEM images showing two homemade AFM tips after engagement. 27

INTRODUCTION

The use of metallic materials (e.g., 430 SS, Crofer 22 APU, and Haynes 230) for SOFC interconnect becomes feasible and attractive as the cell operating temperatures is reduced from 900-1000ºC down to 600-800ºC. The advantages of metallic over ceramic interconnects are obvious: lower material and fabrication costs, easier and more complex shaping possible, better electrical and thermal conductivity, and much less probability of deformation or mechanical failure due to the different gas atmospheres across the interconnection.[1,2] However, it is found that one primary suspected cause of long-term performance degradation of SOFCs is the accumulation of Cr species at and near the cathode/electrolyte interface.[3,4,5,6,7]

Numerous studies have shown that rapid degradation in cathode performance occurs when chromia-containing alloys are used as interconnects, and that several types of Cr species are observed in triple-phase boundaries (TPBs), the regions where the cathode, electrolyte, and oxygen meet.[8,9,10,11,12,13,14,15,16,17,18] Because the TPBs are typically far away (hundreds to thousands of micrometers) from the metal interconnect, it is suspected that the high partial pressure of oxygen and some water vapor in the cathodic compartment lead to the formation of volatile Cr oxides and oxyhydroxides [CrO_3 and $Cr(OH)_2O_2$] from the protective Cr_2O_3-containing film on metal interconnects.[19] These species then diffuse throughout the cathode compartment, leading to deposition of solid Cr_2O_3, most readily in regions where there is a low partial pressure of oxygen, a reducing environment, and the means to remove electrogenerated oxygen anions (O^{2-}). Because the highest rate of oxygen consumption occurs at the TPB of an active cathode, with concurrent production of oxygen anions, it would be logical to assume that the highest concentration of deposited Cr_2O_3 would be at the TPB. Not only would this reaction compete with the electrochemical reduction of oxygen, but it would also result in the deposition of solid species that would block further reduction of oxygen gas at these sites.

These results are mostly based on SOFCs with Sr-doped lanthanum manganite (LSM) cathodes and yttria-doped zirconia (YSZ) electrolyte; the Cr poisoning effect depends on both cathode and electrolyte materials. Matsuzaki and Yasuda studied the electrochemical performance of $La_{0.6}Sr_{0.4}Co_{0.2}Fe_{0.8}O_3$ (LSCF)/$Ce_{0.8}Sm_{0.2}O_{1.9}$ (SDC) assembly under Cr vapor, and found there was no significant Cr poisoning even in the presence of chromium oxyhydroxide vapor at 650 to 900ºC.[20] A possible explanation might be the different overpotentials of the reduction of the cathodes for the oxygen and H_2CrO_4 reduction. While for the manganites the reduction of the chromium oxyhydroxide is the energetically preferred reaction, in the presence of the ferrites the reduction of oxygen appears to require less activation energy. Most recently, Stimner and Stevenson in PNNL [3,21] reported that LSM is more susceptible to Cr evaporation due to low reactivity (and hence high overpotential) for oxygen reduction. Thus, the degree of degradation in cathode performance due to Cr-poisoning follows the order of LSM>LSF>LSCF because LSCF and LSF may gather more Cr and hence reduce the amount of Cr vapor migration to the cathode-electrolyte interface.

A good overview of many issues associated with metallic interconnects is provided by Quadakkers et al.[22] To date, electrochemical polarization, impedance spectroscopy (EIS), Energy dispersive X-ray spectroscopy (EDX), wavelength-dispersive X-ray spectroscopic

(WDX) and high-temperature XRD have been used to study the degradation mechanisms associated with Cr poisoning.[23,24] EDX can only do post-test, not *in situ*, examination of Cr distribution. High-temperature XRD is capable of providing information about phase change under *in situ* conditions; but is sensitive only to crystalline phases, not to glassy or amorphous phases. Also, because of the large penetration depth of x-ray, it is not very sensitive to surface or interfaces.

While considerable efforts have been devoted to the characterization of cathodes exposed to Cr sources, little progress has been made because a full agreement of the chemistry and electrochemistry relevant to the Cr-poisoning processes has not been reached between researchers. The objective of this study is to gain a profound understanding of Cr-poisoning mechanism of the cathode in an operating SOFC and ultimately to establish the scientific basis for achieving rational design of Cr-tolerant cathode materials and structures for low-temperature SOFCs with Cr-based interconnect materials. More specifically, the scientific objectives are:

- To probe and map chromium (Cr) –containing **species/phases** formed at cathode-electrolyte interfaces using various ***in situ* characterization techniques** performed on cathode samples with controllable amounts of electrode and electrolyte surfaces as well as cathode-electrolyte interfaces (composite or patterned electrodes) that are easily accessible to *in situ* electrochemical and optical (Raman) characterization techniques;

- To deduce the **detailed mechanism** for *transport* of Cr-containing gases species, *deposition* of Cr-containing solids in the cathodic compartments (especially at the cathode/electrolyte interface), and the mechanism for the *degradation in performance* of cathodes in SOFCs;

- To correlate Cr contamination delivered by vapor phase Cr-containing molecules and the electrochemical charge transfer resistance of the cathode;

- To **quantitatively characterize** the Cr-related electrochemical degradation, *in situ*, under different ***chemical*** (temperature and partial pressure of Cr-containing gases) and ***electrochemical conditions*** (applied current or voltage);

- To establish **scientific principles** for rational design of better cathode/electrolyte interface (both materials and structures) to minimize or eliminate Cr-related degradation in performance of SOFCs.

This project applies multiple characterization methods – including various Raman spectroscopic techniques and various electrochemical performance measurement techniques – to elucidate and quantify the effect of Cr-related electrochemical degradation at the cathode/electrolyte interface. Raman spectroscopy, which can follow the deposition of Cr-containing phases/species relevant to Cr-poisoning as it happens under *in situ* conditions, is essential to identification of the mechanism of Cr contamination during fuel cell operation. Coupling Raman spectroscopy with *in situ* electrochemical measurements helps directly correlate the surface chemistry with the electrochemistry relevant to Cr-poisoning of cathode.

EXECUTIVE SUMMARY

To make solid oxide fuel cells (SOFCs) more economically feasible, current SOFC research has focused on designing systems and creating materials that would allow the fuel cell to be operated at temperatures below 800ºC. With such lower temperatures, cheaper interconnect materials (such as stainless steels) could be used in SOFC stacks, in lieu of their exotic ceramic counterparts at higher operating temperatures. Research has shown though that associated with these metallic interconnects is a degradation of cell performance brought on by the formation of chromium (Cr) compounds within the SOFC cathode.

The conventional view holds that $CrO_2(OH)_2(g)$, which is present downstream of chromium containing interconnects, is reduced electrochemically at the triple phase boundary (TPB) – the intersection of gas, cathode, and electrolyte phases – to precipitate Cr_2O_3 by the following reaction:

$$2CrO_2(OH)_2(g) + 6e^- = Cr_2O_3(s) + 3O^{2-}(g) + 2H_2O(g)$$

However, Cr-containing contaminants – such as Cr_2O_3, (La, Sr)(Cr,Mn)O_3 or (Cr,Mn)$_3O_4$-type spinel – have been observed *ex situ* on the electrolyte, within the cathode, and on the cathode surface. With results and conclusions varying from paper to paper, no general consensus has been reached on whether the contamination process is chemically- or electrochemically-driven, or whether it occurs through a solid state or vapor phase pathway.

This project uses Raman microspectroscopy, a form of vibrational spectroscopy, to observe the formation of Cr contaminants on SOFC cathode materials under operating conditions. Our unique *in situ* spectroscopy setup allows us to directly identify what compounds are forming as well as which milieux (e.g., cathode surface, electrolyte surface, cathode/electrolyte interface) is more prone to contamination. The samples used were either composites created from mixtures of cathode and electrolyte powder or micropatterned cathodes deposited upon electrolyte substrates. These samples with controlled geometries were placed within a temperature- and atmosphere-controlled sample chamber and exposed to humidified air that had blown over a Cr_2O_3 source to create a Cr-containing vapor. Raman spectra were collected as a function of time, atmosphere, and location to monitor the Cr contamination process.

These *in situ* Raman measurements revealed the formation of $SrCrO_4$ and possibly $(Mn/Cr)_3O_4$ on the surface of LSM within 24 hours exposure to Cr vapor at temperatures as low as 625ºC. No significant amounts Cr-containing contaminants were found on the electrolyte surface. The Cr vapor thus reacts chemically with LSM, covering the cathode and reducing its active surface area. Also of note was the rapid formation of silver chromate (Ag_2CrO_4) in samples utilizing silver wire, silver paste, or silver counterelectrodes. Since Ag_2CrO_4 melts at ~660ºC, it has a significant vapor pressure under normal SOFC operating conditions. The Ag_2CrO_4 selectively deposited on the LSM near the silver source instead of on the YSZ. This deposit demonstrated that LSM is also susceptible to secondary Cr contaminants besides those directly reacting with LSM.

Attempts were made to increase the sensitivity of our Raman measurements by increasing the Raman scattering from the sample through placing metal nanoparticles on the sample surface (surface enhanced Raman scattering, or SERS) or through bringing an AFM tip coated in silver nanoparticles close to the sample surface (tip enhanced Raman scattering, or TERS). SERS measurements with silver nanoparticles were unsuccessful for monitoring Cr contamination since the silver particles themselves easily react with chromium. Gold nanoparticles may still prove practical for SERS measurements. While we developed a method for producing nanoscale silver-coated tungsten AFM tips for TERS measurements, problems with the AFM controller have prevented successful testing of these tips during this phase of the project.

Unlike the LSM samples, the Pt-YSZ composite did not reveal any new Raman signals under *in situ* conditions, even after 120 hours of exposure to the same Cr contamination conditions of the LSM samples. The lack of contaminants on the platinum surface (not even Cr_2O_3) indicates that the presence of the manganese or strontium in LSM is necessary for the creation or adsorption of Cr contaminants.

Overall, we have demonstrated the utility of Raman mapping in monitoring Cr contamination on SOFC cathodes. We present here the first direct *in situ* spectroscopic evidence of the formation of compounds such as $SrCrO_4$ and Ag_2CrO_4 on the surface of LSM. Since the observed Cr contamination appears to be chemically driven, new cathode materials, free of strontium and manganese, are preferable for lower temperature SOFCs being operated in conjunction with Cr-containing interconnect materials.

EXPERIMENTAL

Standard Raman measurements

This project centers around coupling standard electrochemical performance measurements with our unique *in situ* Raman spectroscopy experimental setup to map the concentration of Cr-containing species on the electrode surface as a function of cell operating conditions. Raman spectroscopy identifies the various chemical species in the system by measuring the way in which the sample inelastically scatters an incident laser light signal. By using a microscope and motorized stage to direct the laser light, we can map the chemical environment on and around the cathode/electrolyte interface. Figure 1 shows the experimental setup used for our *in situ* Raman experiments. A Renishaw RM-1000 Raman microscope was used for measuring all Raman spectra. The visible light source was a 25 mW 514 nm laser beam from a Melles Griot Argon Ion laser source. A 50X microscope objective focused the beam down to a spot of ~1 μm diameter on the sample surface. All *in situ* measurements were taken from a sample mounted within a temperature- and atmosphere-controlled sample chamber (special order, Harrick Scientific). To generate a Cr-containing vapor, Cr_2O_3 particulates were placed within in the sample chamber near the gas inlet. The incoming oxygen gas was routed through a bubbler heated to 80ºC and then through heated tubing before entering the chamber. For *in situ* Raman measurements, the samples were heated to the desired temperature and Raman spectra were collected regularly from the electrolyte and cathode phases while the sample was exposed to Cr-containing. Additional *ex situ* Raman spectra were collected upon cooling the sample for comparison with the at-temperature spectra.

While the ultimate spatial resolution of our Raman microscope is 1 μm, the Gaussian intensity distribution of the laser spot allows for detection of phases within ~5 μm of the focused beam. With this limitation, samples must be created with at least 10 μm wide regions of cathode and electrolyte so that any Cr contamination can be independently monitored on both phases. To more easily probe the cathode and electrolyte phases, two types of samples were created, as shown in Figure 2. First, composite cathodes (primarily GDC/LSM) were constructed with dense, well-defined surface structures, and the boundary length vs. surface area were quantified with scanning electron microscopy (SEM). Each polycrystalline GDC and LSM phase were at least 10 microns in diameter. Second, standard microelectronic fabrication methods were used to deposit micropatterned LSM electrodes on a YSZ substrate. The LSM electrodes were at least 10 μm wide and spaced at least 10 μm apart.

Enhanced Raman scattering measurements

In order to detect extremely small amounts of Cr species on the surface, the Raman signal can be enhanced through either deposition of metal nanoparticles on the cathode surface (surface enhanced Raman signal, or SERS) or by bringing a nano-sized metal scanning tip near the cathode surface (tip enhanced Raman signal, or TERS). The increased sensitivity through SERS or TERS methods will allow for earlier detection of deposited Cr species on the sample.

SERS is among the most sensitive techniques available to surface science. Its capability of delivering specific chemical identification and to couple this with a wide range of instruments, has led to its continuing use in both new and traditional areas of surface science. SERS enhancement could be as high as 15 orders of magnitude, which even enable

us to study the Raman spectroscopy of the single molecule[25]. However, the application of this unique surface characterization technique to SOFCs is yet to be developed. To detect layers of Cr_2O_3 below the detection limit of normal Raman measurements, we have attempted incorporation of Ag or Au nanoparticles into the cathode. The nanoparticles have been introduced so far through three different methods (see Figure 3): (1) the evaporation of Ag or Au colloids placed on the cathode surface, leaving behind the nanoparticles within the colloid, (2) the creation of nano-sized Ag or Au islands on a cathode surface by heat treatment of thin sputtered metal films and (3) the co-deposition of Ag nanoparticles with the cathode upon an electrolyte substrate using CCVD.

Work has also been completed towards increasing Raman sensitivity through the TERS effect. Instead of placing metal nanoparticles directly on the cathode surface, a silver-coated AFM tip is brought within a few nanometers of the cathode surface, close enough to obtain a signal enhancement effect. To this end, we finalized a process for manufacturing silver-coated tungsten tips with diameters ranging from 30 to 300 nm. We are currently integrating the AFM control apparatus with our Raman experimental chamber so that we can measure the ability of these tips for creating a significant TERS effect.

RESULTS AND DISCUSSION

Initial *ex situ* Raman experiments

The first round of Raman measurements involved demonstrating the utility of normal Raman spectroscopy (measurements without signal enhancements) with respect to Cr contamination of an LSM cathode. As shown in Figure 4, the Raman signals from possible chromium-containing contaminants are different from that of the LSM cathode, meaning Raman spectroscopy can indeed distinguish between the multiple species present. For example, the sharp peaks at 350 cm^{-1} and 550 cm^{-1} in the spectrum of Cr_2O_3 can be used as a marker in contrast with the relatively flat spectrum of the LSM. For each desired species, an algorithm has been created to quantify the intensity of the Raman signal from the specific species. Raman maps can thus be created from our samples that plot the Raman signal from a desired species as a function of position. Figure 5 shows an example of a Raman map of Cr_2O_3 on LSM.

In situ Raman experiments

For the first *in situ* measurements, LSM-GDC composite cathode samples (co-pressed and co-sintered with a GDC electrolyte and with a silver counter electrode) were used. The sample was heated to 650ºC within the chamber and the dry air inlet gas was routed through a heated bubbler. The humidified air increased the volatility of the Cr_2O_3 placed inside chamber near the composite cathode sample. A mass spectrometer was attached to the exhaust gas line to analyze the chamber atmosphere; however, no Cr-containing species were detected. This result was expected as the baseline noise for the instrument is on the order of 10^{-8} atm, while the vapor pressure for most Cr species at 650ºC is expected to be 10^{-9} atm or less.

Of the two composite samples tested, only one was able to be polarized. The other sample shorted out after being held at temperature for a few hours. The sample that was polarized also eventually shorted after six hours of polarization. During these six hours, the bulk resistance of the cell linearly decreased from ~100 Ω down to a nominal 1 Ω, the resistance of the lead wires. The optical microscope revealed cracks in the cathode surface, which may have penetrated through the entire sample and allowed the silver paste used to connect the lead wires to the cathode to flow through the sample and make contact with the counter electrode. Similarly, the lead wire was attached closed to the edge of the pellet, so the silver paste may simply have flowed over the edge of the sample down to the other side. Overall, both samples were exposed to humidified air in the presence of Cr_2O_3 at 650ºC for 36 hours before cooling the samples down. Raman spectra collected *in situ* from the cathode surface during this time developed no new peaks, as shown in Figure 6.

While we measured no new peaks on the composite cathode surface during the initial *in situ* measurements, upon cooling the sample and removing it from the chamber, a slight red discoloration was observed on the silver electrode on the reverse side of the sample. Raman spectra collected from this bottom surface did change significantly during the experiment. Figure 7 shows Raman spectra collected from the silver surface of the sample that had not been polarized from before the experiment and from after the sample had been cooled to room temperature. The spectra have been normalized for easier comparison; however, it should be noted that the new peaks that emerged around 650 and 820 cm^{-1} (two separate series of overlapping peaks) have a signal that is over one order of

magnitude greater than the signal from the silver before the experiment. For the sample that had briefly been polarized, the discoloration of the silver counterelectrode was more defined, and the newly-developed Raman peaks near 820 cm^{-1} were more intense. New peaks near 810 cm^{-1} were also observed from the GDC electrolyte surface near the Ag electrode, as shown in Figure 8.

SEM analysis of the silver electrode revealed the presence of faceted grains embedded with the silver paste. EDS elemental analysis of the sample confirmed the presence of chromium within these grains. Further EDS analysis revealed the presence of chromium not only on the surface of the silver electrode, but also on the GDC electrolyte near the silver electrode. The presence of chromium on the silver electrode and GDC electrolyte surface confirms that the experimental setup indeed created Cr-containing vapor within the chamber. The correspondence between the presence of the chromium with silver led us to conclude that what was forming on the sample was Ag_2CrO_4, which is red in color. Figure 8 shows the match between the Raman spectrum for Ag_2CrO_4 with that of the red deposit on the composite sample. The broader nature of the peaks from the deposit compared to pure probably results from a highly defective structure in the deposit. The melting point of Ag_2CrO_4 is ~660ºC, so the Ag_2CrO_4 that formed on the sample was deposited in a near-liquid state. The secondary peak at 650 cm^{-1} could also be a result of a disordered Ag_2CrO_4 structure; however, no definitive peak assignment has been given to that peak yet.

These results were corroborated by measurements taken under similar conditions using a micropatterned LSM electrode sample. The micropatterned sample had a silver counterelectrode painted underneath, and a patterned platinum current collector had been deposited over the LSM pattern. Silver wire (to connect the sample to the electrochemical interface) was run through the quartz window of the sample chamber and attached to the platinum current collector using silver paste. The sample was heated to 625ºC and exposed to humidified air containing Cr vapor. The sample was exposed first without polarization to monitor any chemical reactions (as opposed to electrochemical) between the Cr vapor and the sample. With 100 hrs, a red deposit could be seen visually *in situ* where the silver wire was connected to the LSM pattern, shown in Figure 9(b). After three weeks exposure the red deposit could be clearly seen not only on the silver wire, but also on the LSM electrode (see Fig. 9(c)), up to 500 μm away from the silver wire.

Figure 10 contains Raman spectra collected from various surfaces of the sample. The Ag_2CrO_4 phase could be detected on the silver wire and also on the LSM electrode and Pt current collector near the wire, but no signal was observed on the YSZ electrolyte. To confirm the distribution of Ag_2CrO_4, the Raman map in Figure 11 was created by plotting the intensity of 810 cm^{-1} Ag_2CrO_4 peak as a function of position. The Ag_2CrO_4 phase preferentially deposited on the LSM and Pt surfaces.

The presence of the Ag_2CrO_4 and the milieux where it formed are of interest to the study of Cr contamination. First, while silver is not used in current SOFC systems, some recent investigations have been made into its introduction in intermediate temperature SOFCs (IT-SOFCs) operating below 800ºC. Since Ag_2CrO_4 melts at 660ºC, its formation and properties are of great concern for IT-SOFCs that operate between 500ºC and 700ºC. With silver reacting so quickly with Cr, it could act as a buffer between the Cr-containing interconnect and an LSM cathode. However, this benefit is counterbalanced with the volatility of Ag_2CrO_4, as the Ag_2CrO_4 will deposit on the LSM surface, causing a reduction in active electrode surface area. Further, as Ag_2CrO_4 forms and vaporizes, the electrical contact

between the silver and interconnect will be lost. Second, the fact that the Ag_2CrO_4 formed preferentially on the LSM (and secondarily on the platinum current collector) indicates that LSM (or a metal such as platinum) may play an important in Cr poisoning, even without the presence of silver to form Ag_2CrO_4. While LSM is a necessity for the formation of the $(MnCr)_3O_4$ spinel or $SrCrO_4$ often found in Cr-poisoned cathodes, it may not be necessary for the deposition of Cr_2O_3. Further, if Ag_2CrO_4 deposited on LSM through only chemical exposure, Cr_2O_3 could also deposit chemically throughout the cathode.

The possibility of chemically-driven Cr contamination was thus further tested using a micropatterned LSM sample that did not contain silver wire or paste. A patterned sample without a counterelectrode or attached wires was heated to 625ºC and exposed to humidified oxygen blowing over a Cr_2O_3 source. The *in situ* Raman spectrum in Figure 12(a) shows that even within 24 hrs, a new peak at 875 cm^{-1} began to emerge. The signal strength did not drastically increase within the next 24 hours, so the sample was cooled to room temperature and examined *ex situ*. The peaks in the room temperature spectra (see Fig. 12(b)) were sharper and much more intense. This is a common effect, as lattice expansion and increased nonstoichiometry at higher temperature causes peaks to broaden and to shift to lower frequencies. After comparison with reference Raman spectra, the family of peaks near 875 cm^{-1} and below 400 cm^{-1} were assigned to $SrCrO_4$, a reported possible Cr-containing contaminant. The room temperature peaks at 660 cm^{-1} and 570 cm^{-1}may correspond to some composition of the $(Mn/Cr)_3O_4$ spinel. These peaks were not observed *in situ*, so the phase may have formed during cooling. However, the phase may be present at elevated temperatures, but the peaks may become too broad and weak to quickly detect with our current system.

The authors believe this is the first reported *in situ* evidence of the formation of a Cr contaminant on the surface of an LSM cathode. Since no current was passing through the cell, its formation appears to be chemically-driven. To see whether this contaminant was restricted to the LSM phase (which it would be if it were $SrCrO_4$), an *ex situ* map was created by plotting the integrated intensity of the 875 cm^{-1} peak from the region of the patterned LSM sample shown in Figure 13. As with the Ag_2CrO_4 from the Ag-containing patterned sample, the contaminant formed almost exclusively on the LSM electrode. Not only does LSM act as a chemical source for chromium contamination (in the case of $SrCrO_4$), it also seems to be a catalytically-active formation or adsorption site for Cr-containing oxides.

The chemical contamination of LSM by chromium vapor was further tested by exposing a pellet of pure LSM to Cr-containing gas at 625ºC. Figure 14(a) contains a Raman spectrum collected after 24 hours exposure to Cr vapor that contains the 875 cm^{-1} peak observed with the patterned LSM sample. Cooling the sample once again revealed Raman peaks centered around 900 and 400 cm^{-1}, as well as at 660 cm^{-1}, although the relative intensities of the peaks were different. These variations could be caused by the differences in the two LSM sources (i.e., a dense, fired pellet compared with a sputtered thin film). Additional characterization methods (e.g., XRD, XPS) should be used to more fully identify the Cr contaminants forming on the LSM surface.

To test whether LSM is necessary for the creation or adsorption of Cr contaminants, a composite sample of platinum and YSZ was exposed to the same Cr contamination conditions of the LSM samples. Unlike the LSM samples, the Pt-YSZ composite did not reveal any new Raman signals under *in situ* conditions, even after 120 hours of exposure

(see Figure 15). The lack of contaminants on the platinum surface (not even Cr_2O_3) indicates that the presence of the manganese or strontium in LSM necessary for Cr contamination. Ideally, cathode materials should be chosen that do not contain these cations.

Enhanced Raman scattering experiments

SERS experiments

The sensitivity of the Raman microscope to the presence of Cr_2O_3 was determined by sputtering thin Cr_2O_3 films of varying thicknesses onto LSM samples and measuring the Raman signal. As shown in Table 1, films as thin as 10 nm could be detected, even without signal enhancements. To detect extremely thin layers of Cr_2O_3 (< 10 nm), we have attempted incorporating of Ag or Au nanoparticles into the cathode, which has been shown to increase the Raman signal from the volume around the nanoparticles through a phenomenon known as the SERS effect. The nanoparticles were introduced initially through two different methods: (1) the evaporation of Ag or Au colloids placed on the cathode surface, and (2) the co-deposition of Ag nanoparticles with the cathode upon an electrolyte substrate using CCVD. Both of these methods produced varying degrees of success, increasing the Raman signal from LSM or Cr_2O_3 by a factor between 5 and 1000, depending on the technique and the material. Specific peaks within a given Raman spectrum were enhanced by different amounts, and previously undetected peaks have also appeared with the addition of the metal nanoparticles. Figure 16 shows the SERS effect generated from a Cr_2O_3 film that was prepared by CCVD with and without the presence of Ag nanoparticles. Adding Ag nanoparticles using CCVD did increase the intensity of the Raman signal; however, new peaks at 810, 775, and 650 cm^{-1} appeared. These peaks were previously ascribed to Ag_2CrO_4, indicating that the Ag and Cr reacted in the CCVD flame and were deposited as Ag_2CrO_4. Since Ag_2CrO_4 has already been shown to form in a system at 625ºC, silver nanoparticles cannot be used to generate a SERS effect when studying chromium contamination. The silver nanoparticles would quickly react with the Cr vapor and thus lose their ability to produce the plasmon field necessary for scattering intensity enhancement. SERS experiments using Cr_2O_3 with sputtered silver islands or silver colloids revealed similar tendencies to form Ag_2CrO_4 upon heating the sample even above 400ºC. The use of silver nanoparticles for SERS measurements of Cr contamination must thus be limited to *ex situ* measurements. Since gold does not react easily with chromium, it is still a viable option for creating a SERS effect for *in situ* Raman measurements. No SERS experiments using gold nanoparticles were carried out in this phase of the project.

TERS experiments

For high temperature *in situ* TERS to be possible, a homemade tip must be prepared, as the commercial one can't be used at high temperatures. However, the commercial one were used for initial *ex situ* experiments to check the whole system and guide the tip preparation. A sharp tip is essential to achieved tip-enhanced Raman spectroscopy. A two-staged procedure was employed to get sharp tungsten tips of nanometer and subnanometer apex dimensions. Its mechanism is based on bubble dynamics. Tips were etched in NaOH in two slow steps: first, a narrow cone with a fairly blunt tip was produced, and second, the final sharpening was accomplished in a modified configuration in which the wire was immersed pointing upward with an AC voltage. The bubbles were pushed upward by buoyancy as the

etching voltage was negative, and the NaOH solution around the tip flowed upward. Because the tip is also pointing upward, the etching process only polished the tip in the upward direction. The described process suffered from irreproducibility. Since bubbles play a critical role in the second etching process, an increase of period and amplitude of the negative potential was applied to control the bubble generation. Based on this improvement, we greatly improved the reproducibility of the second sharpening step. Shown in Figure 17(a) is a TEM image of a tip covered by one layer of NaOH; the tip diameter is less than 10 nm. Once the tip was prepared and rinsed with steam water and methanol, it was coated by Ag by DC sputtering. Figure 17(b) shows an SEM image a coated W tip.

The tip with Ag coating was attached on the tip mount and applied for TERS. We could not get an enhanced Raman signal. The integrity of the tip was examined to find out the reason for a lack of enhanced Raman signal. Before its initial use in the AFM, the tip was examed using SEM to ensure that it was sharp. As soon as the tip was engaged, it was lifted, detached from the tip mount, and again characterized by SEM. Figure 18 shows that two separate tips tested in this manner were both bent, rendering them useless for TERS.

We are currently communicating with the AFM maker to diagnose the problem and to determine the best method for servicing the AFM. The current problem is believed to be the result of a faulty controller. We are confident that we can once again perform TERS once the AFM has been returned to proper working condition.

CONCLUSIONS

Under the support of this SECA project, we made important progress in elucidation of the mechanism of chromium contamination of cathode materials for SOFCs by means *in situ* Raman microspectroscopy. The following significant conclusions can be drawn from the work completed in this phase of the project:

- If silver is present in the SOFC cathode, it will react quickly with Cr-containing vapor to form Ag_2CrO_4. The silver chromate will then in turn volatize and deposit on an LSM cathode surface. It is the recommendation of this group that careful design consideration must be given to an SOFC that attempts to use silver within the cathode, if used in conjunction with a Cr-containing cell component (e.g., interconnect).
- Even at temperatures as low as 625ºC, Cr vapor can react with LSM to form $SrCrO_4$ (and possibly $(Mn/Cr)_3O_4$) on the LSM surface, as confirmed through the use of *in situ* Raman spectroscopy measurements. This result is especially significant in that this is the first time that the formation of a chromium contaminant has been observed *in situ* on an SOFC cathode surface.
- Due to its reactive nature to Cr vapor, silver nanoparticles cannot be used *in situ* to generate a SERS effect for studying Cr contamination. Gold nanoparticles remain as a possibility for *in situ* SERS measurements.
- Raman spectroscopy (including SERS and TERS) has the potential for *in situ* probing and mapping of Cr species deposited on cathode surfaces in a functional SOFC under practical operating conditions. Even without signal enhancement, Raman mapping of Cr-containing species can be performed on SOFC cathodes for deposits thicker than 10 nm.
- In addition to silver, the Sr and Mn cations appear to be active for chemical reaction with Cr vapor, forming $SrCrO_4$ and $(Mn/Cr)_3O_4$ spinel on LSM. Further, LSM was also shown to be an active site for the deposition of Ag_2CrO_4 for samples that also contained silver.
- In contrast, Pt and YSZ do not appear to be active for formation of Cr-containing phases.
- Results seem to indicate that Cr contamination is predominantly chemically-driven.
- In order to minimize the Cr-contamination effect, cathode materials should be chosen that are free of cations/elements that could preferentially react with chromium, including silver, strontium, and manganese.

The authors recommend further use of Raman microscopy for *in situ* monitoring of SOFC reactions. The following topics would be of particular interest:

- Performing *in situ* Raman mapping of Cr contamination on a polarized electrode to see if, where, and to what extent the contamination process is affected by current flow. These experiments would address any possible electrochemical contributions to the contamination process.
- Development of an *in situ* TERS apparatus for monitoring geography-specific Cr contamination on a sub-micron scale. The higher mapping resolution offered by TERS would allow for more precise characterization of reactions occurring at the TPB, along the electrode/electrolyte interface, and on the electrode surface.

FIGURES AND TABLES

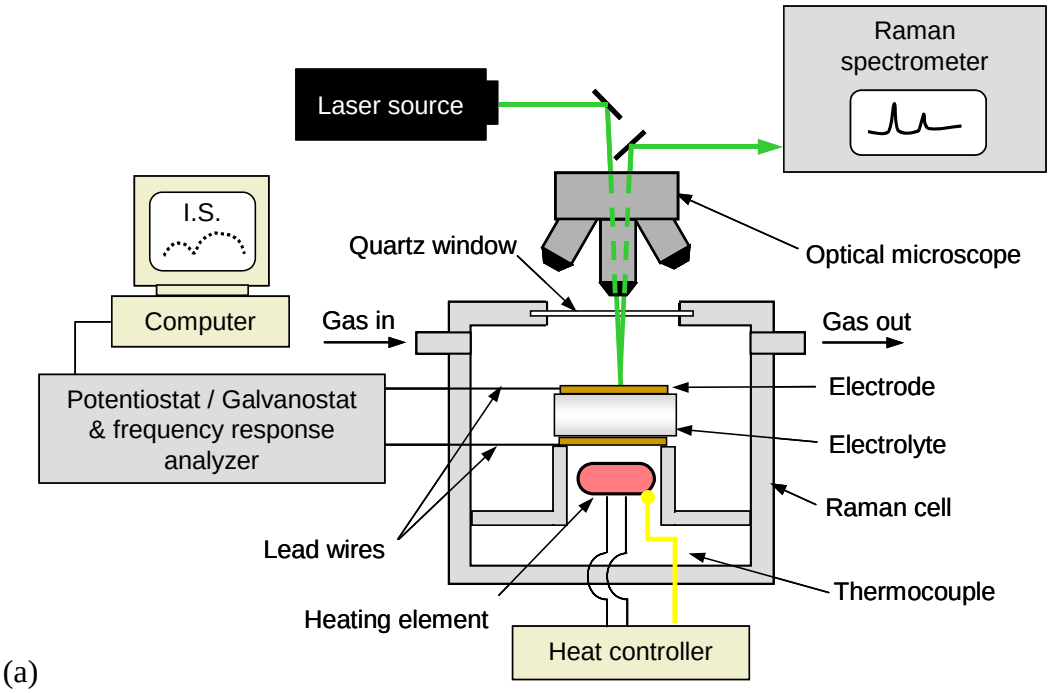

(a)

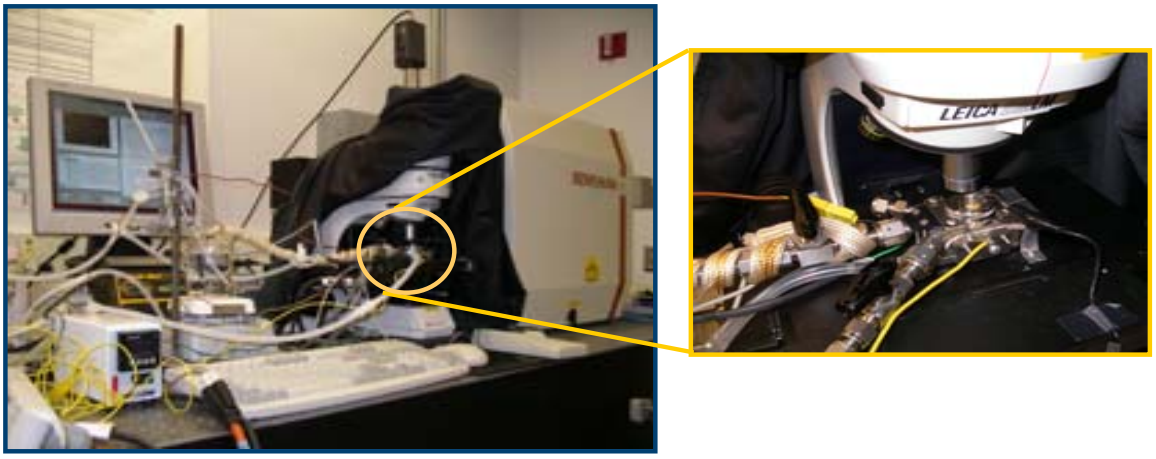

(b)

Figure 1. (a) Schematic and (b) photograph of *in situ* Raman spectroscopy system.

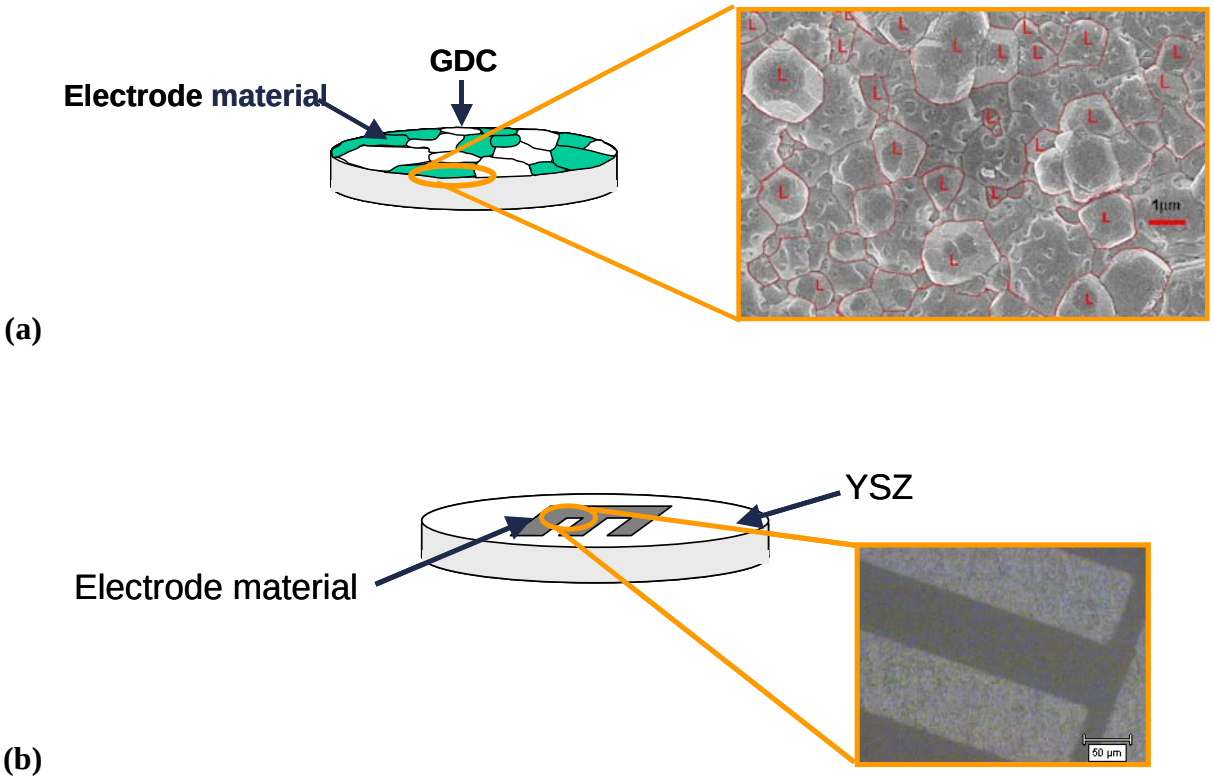

Figure 2. (a) LSM/GDC composite and (b) micropatterned LSM electrode samples used for *in situ* Raman measurements. For the composite sample micrograph, the outlined red regions are LSM.

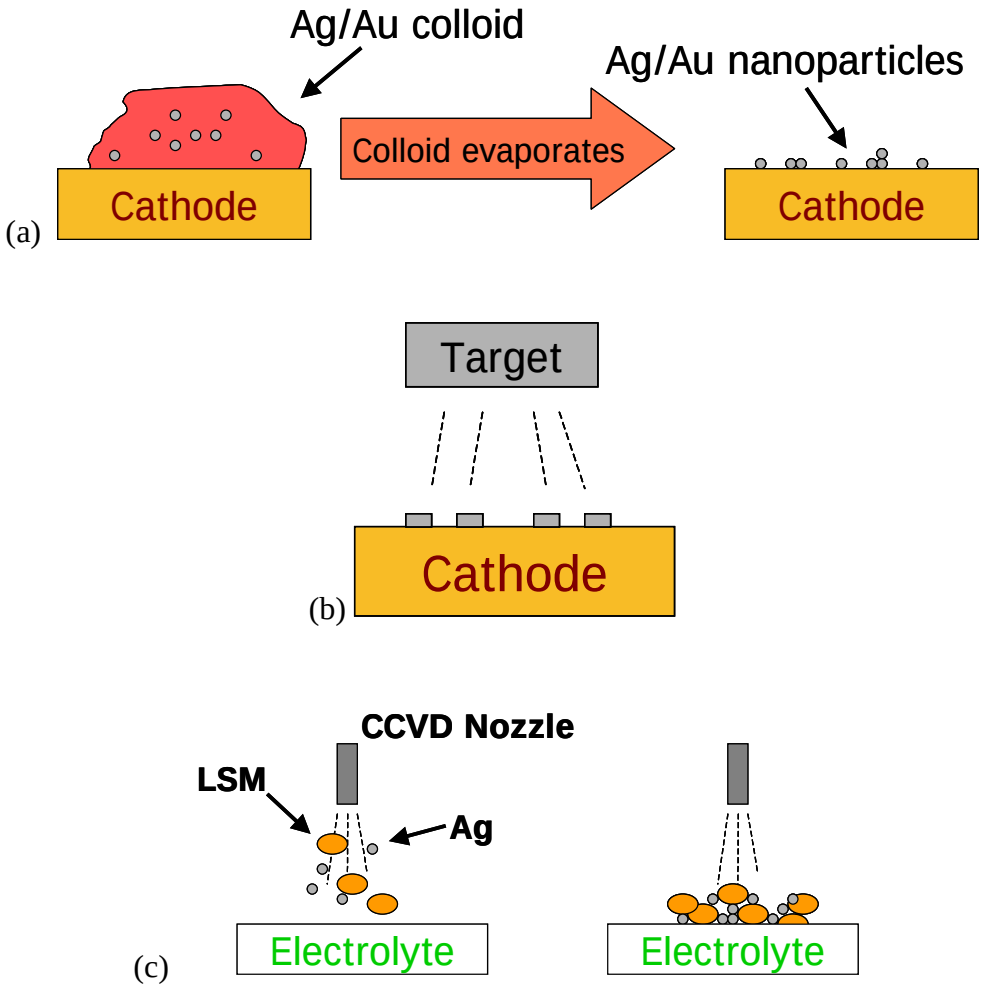

Figure 3. Creation of SERS effect on cathode surface by (a) evaporating Au/Ag colloids on cathode surface, (b) sputtering nano-sized Au/Ag islands on cathode, and (b) co-depositing cathode material along with Ag nanoparticles.

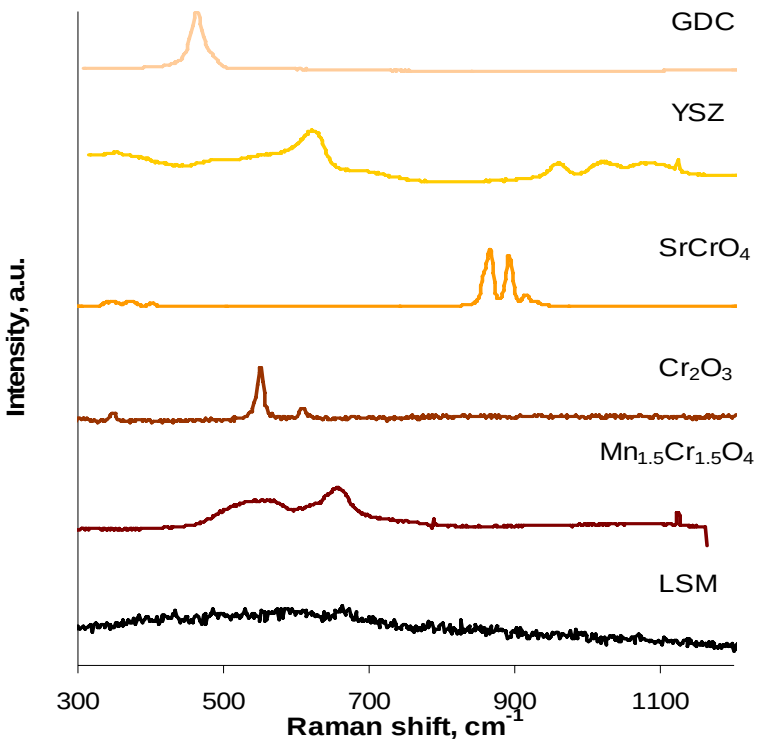

Figure 4. Raman spectra of various chromium-containing phases compared with the Raman spectra of standard SOFC components.

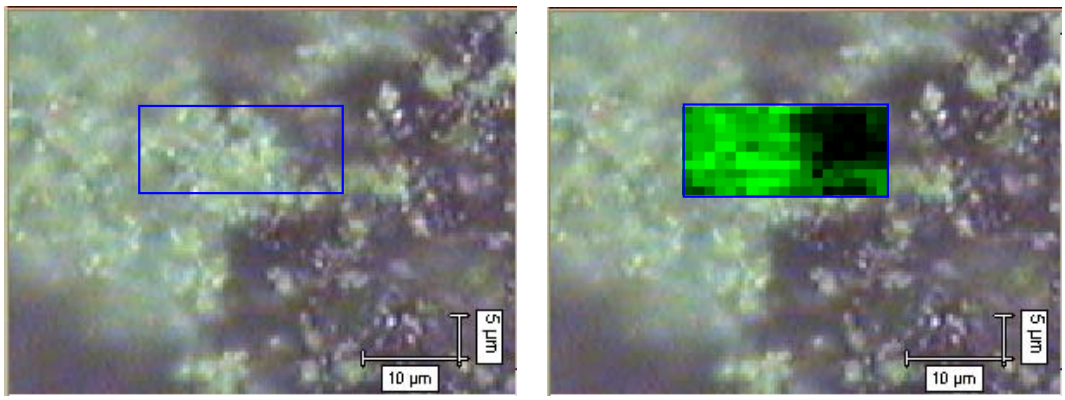

(a) (b)

Figure 5. (a) Microscope image of Cr_2O_3 powder (the light phase) on an LSM substrate (the dark phase). (b) Raman map plotting the intensity of the Raman signal at 550 cm^{-1} as a function of position. The brighter the green, the greater the signal intensity. Each pixel represents 1 μm^2.

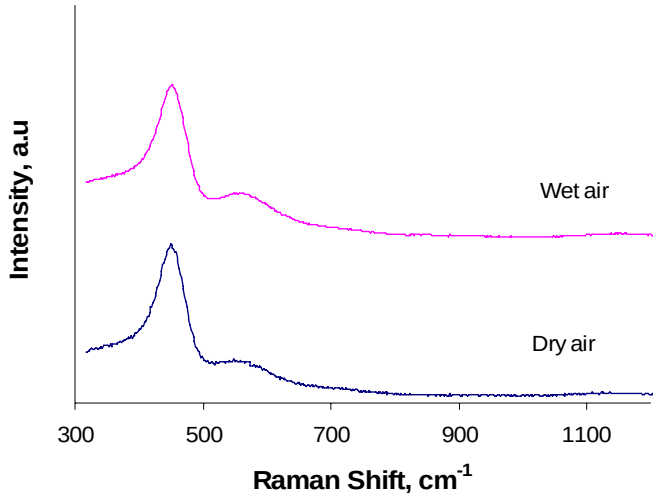

Figure 6. Raman spectra from the LSM-GDC composite surface before and after exposure to humidified air for 24 hours. The spectra were collected at 650ºC.

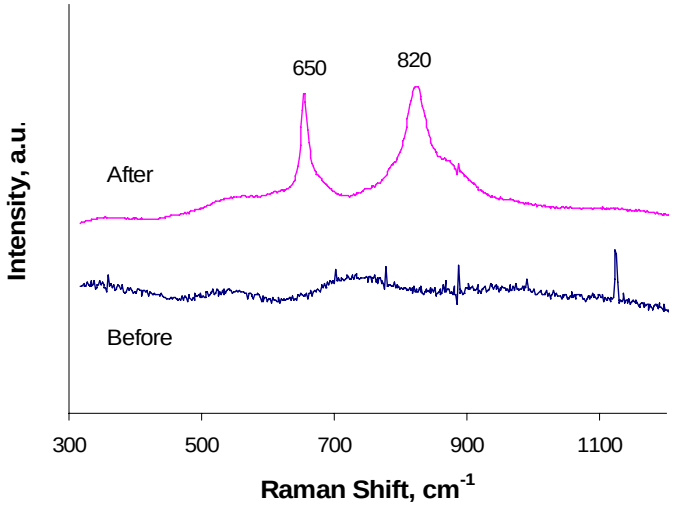

Figure 7. Raman spectra collected from the silver counterelectrode surface before and after exposure to Cr-containing air at 650ºC for 36 hours without polarization. Both spectra were measured at room temperature.

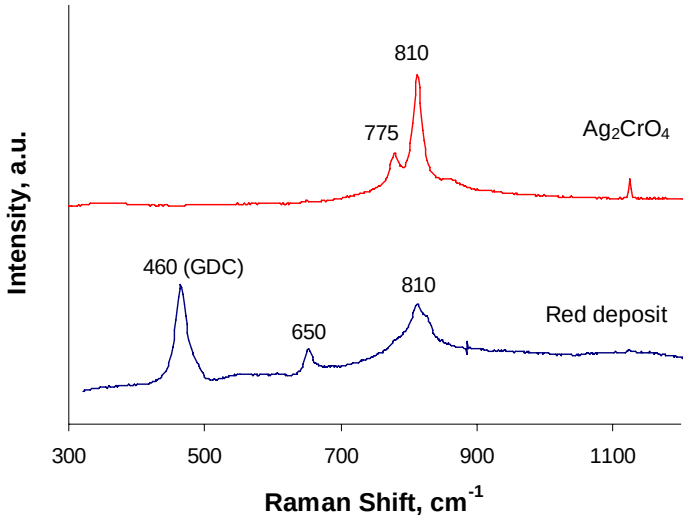

Figure 8. Raman spectra from red deposit on LSM-GDC composite sample and from Ag_2CrO_4 powder.

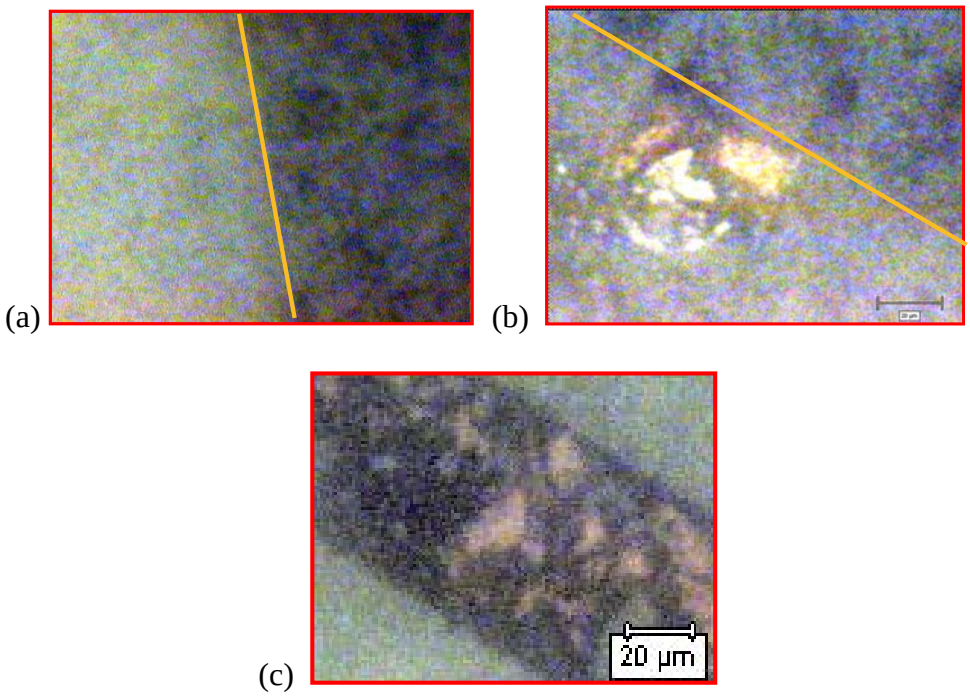

Figure 9. Optical micrographs of micropatterned LSM sample at 625ºC exposed to Cr-containing vapor for (a) 0, (b) 5, and (c) 21 days. The orange line denotes an LSM-YSZ interface. Figure 9(b) shows the contact point between the silver wire and an LSM electrode.

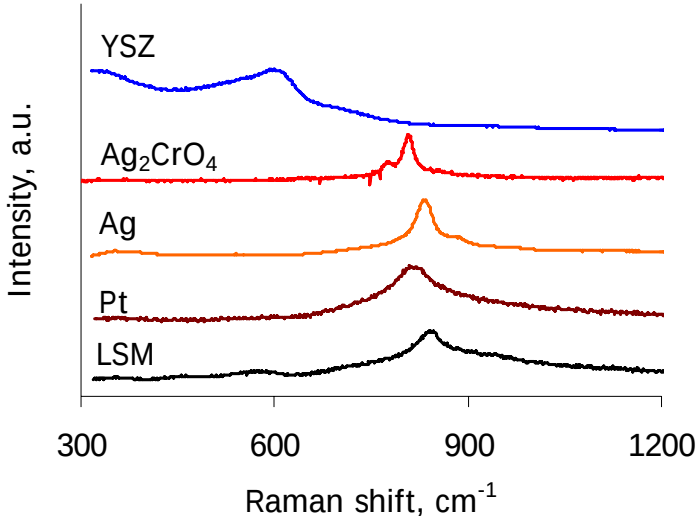

Figure 10. Raman spectra collected *in situ* from the micropatterned LSM sample after exposure to Cr vapor at 625ºC for three weeks.

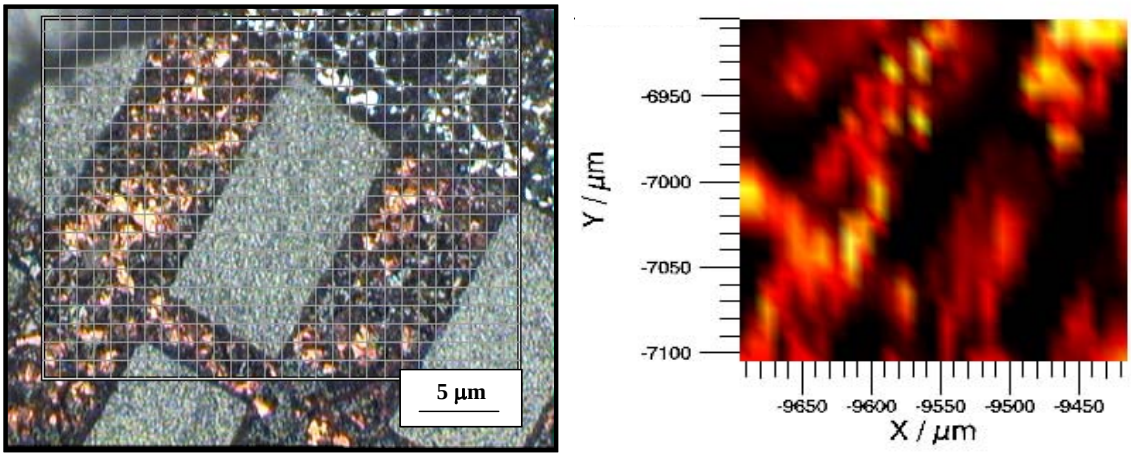

Figure 11. Raman map of Ag_2CrO_4 on a patterned LSM electrode (on a YSZ substrate) after exposure The Raman spectra for the map were collected *ex situ* at room temperature.

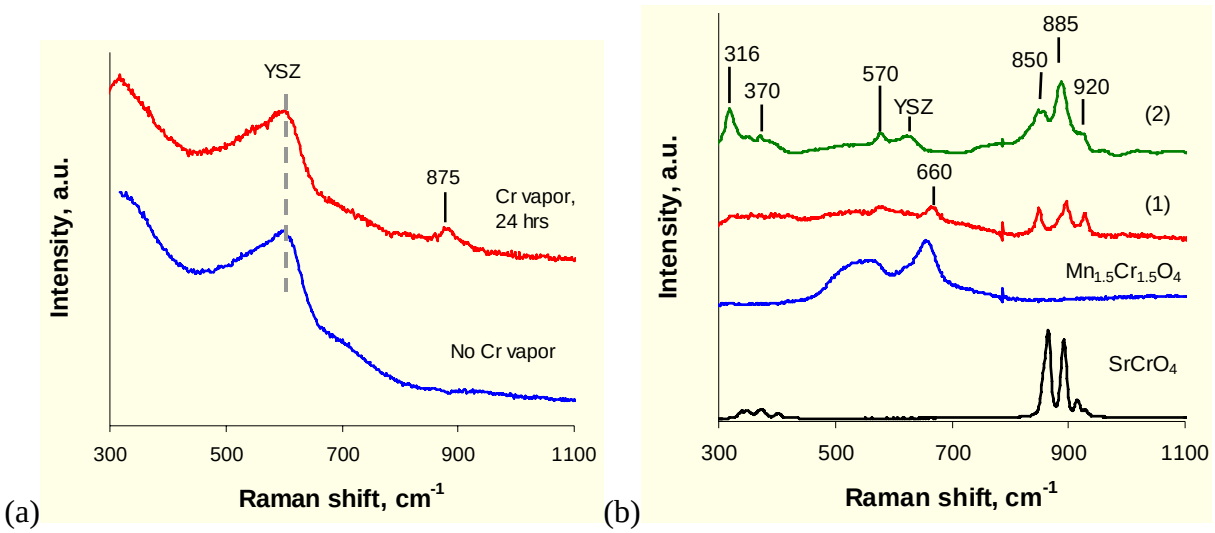

Figure 12. (a) Raman spectra from patterned LSM electrode at 625ºC before and after exposure to Cr-containing humidified oxygen. (b) Spectra (1) and (2) were collected *ex situ* from the sample after 48 hrs exposure to Cr vapor.

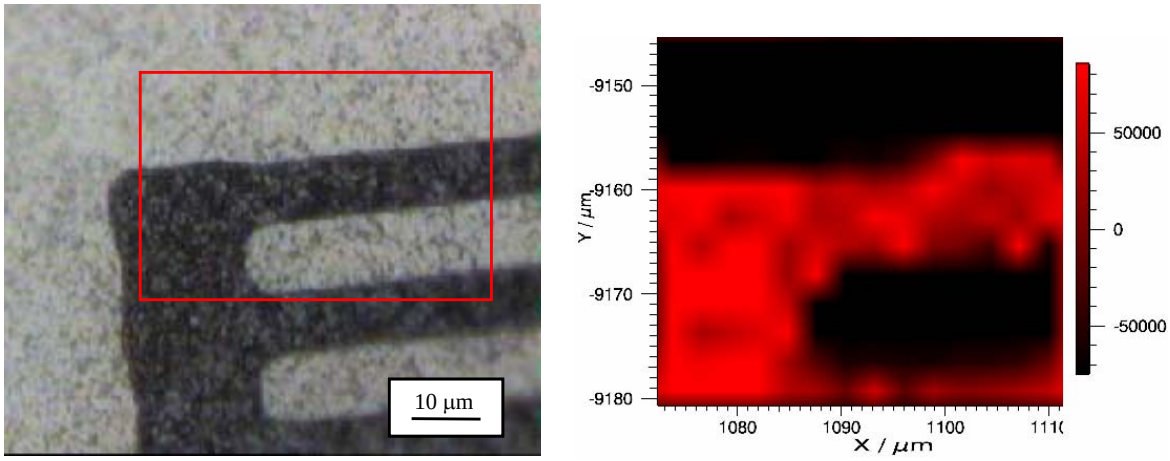

Figure 13. Raman map plotting the integrated intensity of the 885 cm^{-1} peak from $SrCrO_4$ on the micropatterned LSM on YSZ sample exposed to Cr vapor for 48 at 625ºC. The map was generated *ex situ* at room temperature. The red box in the micrograph indicates the map area.

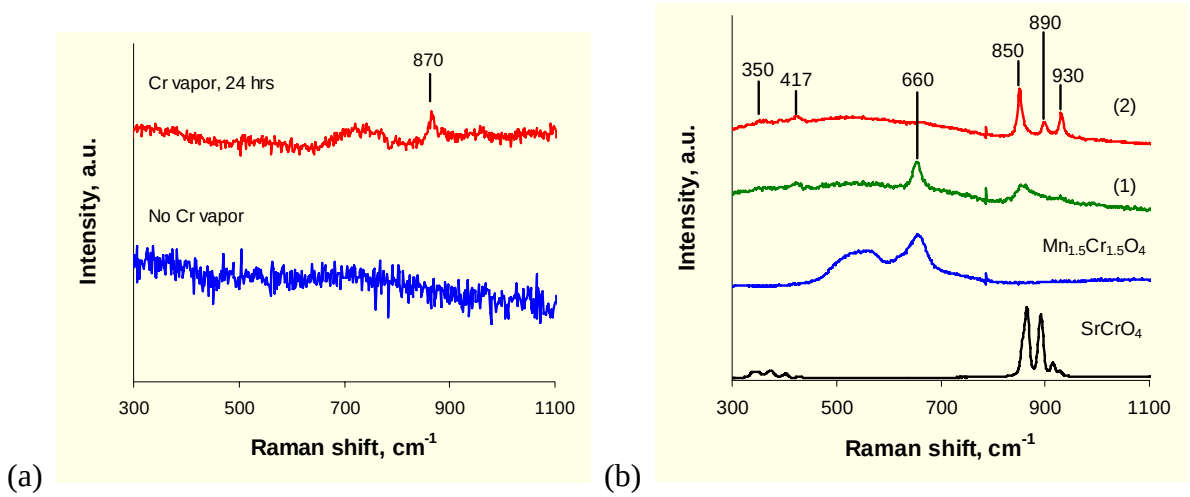

Figure 14. (a) *In situ* Raman spectra from dense LSM pellet at 625ºC before and after exposure to Cr-containing humidified oxygen for 24 hrs. (b) Spectra (1) and (2) were collected room temperature from the same sample.

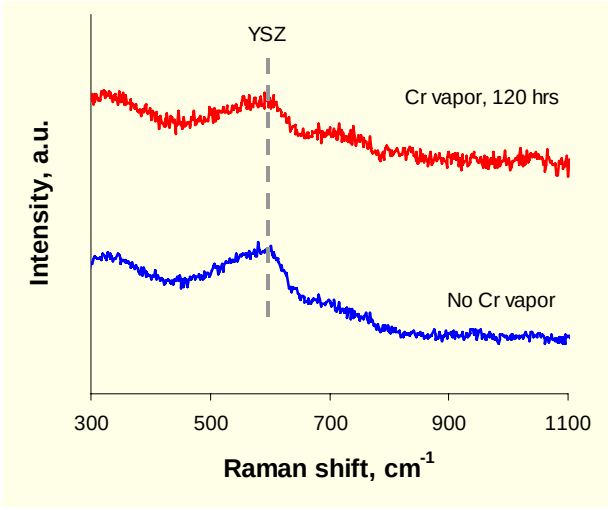

Figure 15. *In situ* Raman spectra from Pt-YSZ composite at 625ºC before and after exposure to Cr-containing Cr vapor for 120 hrs.

Table 1. Comparison of Raman scattering intensity of the 553 cm^{-1} peak from different film thicknesses of Cr_2O_3 sputtered on various LSM-containing substrates

Film thickness, nm	Peak intensity	Intensity normalized to 1.83 μm film
1830	68000	1.000
200	800	0.012
20	60*	0.001

* 20 nm intensity was scaled down to match the measuring time of the other samples.

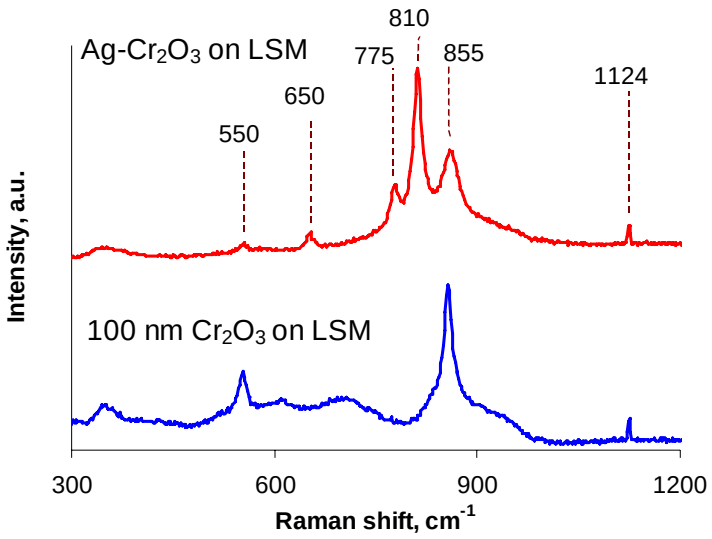

Figure 16. Raman spectra of a Cr_2O_3 film deposited on an LSM substrate using CCVD with and without Ag nanoparticles.

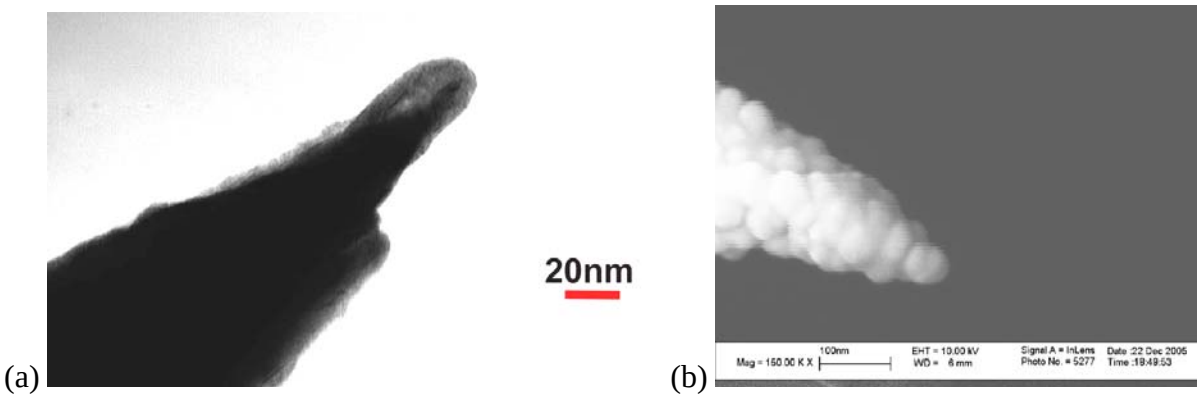

Figure 17. Images of a sharp tungsten AFM tip (a) before and (b) after coating with silver.

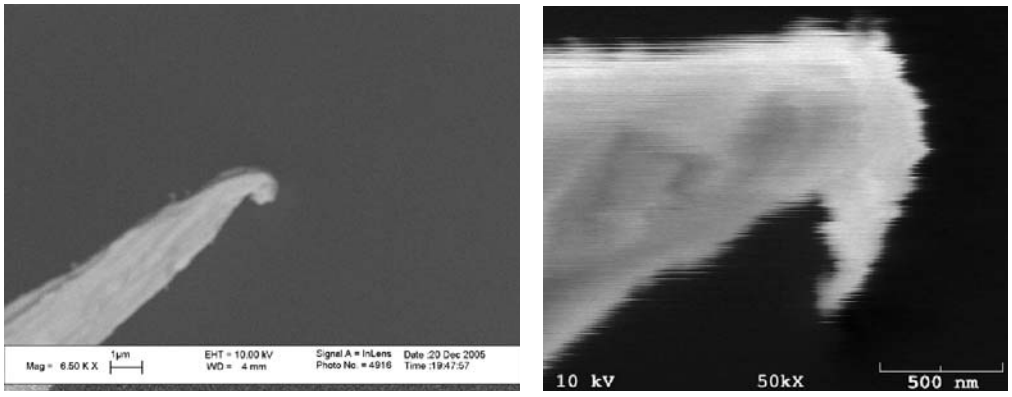

Figure 18. SEM images showing two homemade AFM tips after engagement.

REFERENCES

1. N.Q. Minh, T. Takahashi, in Science and Technology of Ceramic Fuel Cells, Elsevier Science B.V., 1995, p188.

2. S.C. Singhal, K. Kendall, in High temperature **solid oxide fuel cells:** fundamentals, design, and applications, Oxford, New York, Elsevier, 2003, p181.

3. SECA Workshop Proceedings (I – IV) and Core Technology Workshop Proceedings, www.seca.doe.gov .

4. SOFC (I – VIII) Proceedings, ed. Dr. Subhash C. Singhal, Electrochemical Society, www.electrochem.org

5. Proceedings of the European Solid Oxide Fuel Cell Forum (I – VI), Lucerne, Switzerland, www.efcf.com

6. Fuel Cell Seminar Abstracts (1976 – 2004), Courtesy Associates, fuelcell@courtesyassoc.com .

7. SECA Core Technology Program – SOFC Seal Meeting, Albuquerque, NM. July, 2003, http://www.netl.doe.gov/publications/proceedings/03/seca-seal/sofc-seal.html

8. S. P. Jiang, A comparison of O_2 reduction reactions on porous $(La,Sr)MnO_3$ and $(La,Sr)(Co,Fe)O_3$ electrodes. *Solid State Ionics,* **146** (**1-2)**, (2002) 1-22.

9. S. P. Jiang, J. P. Zhang, and X. G. Zheng, A comparative investigation of chromium deposition at air electrodes of solid oxide fuel cells. *J. Eur. Ceram. Soc.*, **22**, (2002) 361-373.

10. S. P. Jiang, Use of gaseous Cr species to diagnose surface and bulk process for O_2 reduction in solid oxide fuel cells. *J. Appl. Electrochem.,* **31**, (2001) 181-192.

11. Y. Matsuzaki and I. Yasuda, Electrochemical properties of a SOFC cathode in contact with a chromium-containing alloy separator. *Solid State Ionics,* **132**, (2000) 271-278.

12. S. P. Jiang, J. P. Zhang, L. Apateanu, and K. Foger, Deposition of chromium species at Sr-doped $LaMnO_3$ electrodes in solid oxide fuel cells I. Mechanism and kinetics. *J. Electrochem. Soc.*, **147**, (2000) 4013-4022.

13. S. P. Jiang, J. P. Zhang, and K. Foger, Deposition of chromium species at Sr-doped $LaMnO_3$ electrodes in solid oxide fuel cells - II. Effect on O_2 reduction reaction. *J. Electrochem. Soc.*, **147**, (2000) 3195-3205.

14. S. P. Jiang, J. P. Zhang, and K. Foger, Deposition of chromium species at Sr-doped $LaMnO_3$ electrodes in solid oxide fuel cells - III. Effect of air flow. *J. Electrochem. Soc.*, **148**, (2001) C447-C455.

15. Y. Larring and T. Norby, Spinel and perovskite functional layers between Plansee metallic interconnect (Cr-5 wt% Fe-1 wt% Y_2O_3) and ceramic $(La_{0.85}Sr_{0.15})_{0.91}MnO_3$ cathode materials for solid oxide fuel cells. *J. Electrochem. Soc.,* **147**, (2000) 3251-3256.

16. S. P. Jiang, J. P. Zhang, L. Apateanu, and K. Foger, Deposition of chromium species on Sr-doped LaMnO3 cathodes in solid oxide fuel cells. *Electrochem. Commun.,* **1**, (1999) 394-397.

17. S. P. S. Badwal, R. Deller, K. Foger, Y. Ramprakash, and J. P. Zhang, Interaction between chromia forming alloy interconnects and air electrode of solid oxide fuel cells. *Solid State Ionics*, **99**, (1997) 297-310.

18. S. Taniguchi, M. Kadowaki, H. Kawamura, T. Yasuo, Y. Akiyama, Y. Miyake, and T. Saitoh, Degradation phenomena in the cathode of a solid oxide fuel cell with an alloy separator. *J. Power Sources*, **55**, (1995) 73-79.

19. Y. Matsuzaki and I. Yasuda, Dependence of SOFC cathode degradation by chromium-containing alloy on compositions of electrodes and electrolytes. *J. Electrochem. Soc.*, **148**, (2001) A126-A131.

20. K. Hilpert, D. Das, M. Miller, D. H. Peck, and R. Weib, Chromium vapor species over solid oxide fuel cell interconnect materials and their potential for degradation processes. *J. Electrochem. Soc.*, **143**, (1996) 3642-3647.

21. S. Simner, M. Anderson, J. Stevenson. La(Sr)FeO_3 SOFC cathodes with marginal copper doping. *J. Am. Cera. Soc.* **87** (2004) 1471-1476.

22. W.J. Quadakkers, J. Piron-Abellan, V. Shemet, L. Singheiser. Metallic interconnectors for solid oxide fuel cells - a review. *Mater. High Temperatures*, **20** (2) (2003) 115-127.

23. M.S. Anderson, Locally enhanced Raman spectroscopy with an atomic force microscope. *Applied Physics Letters*, **76** (2000) 3130-3132.

24. I.E. Wachs, In situ Raman spectroscopy studies of catalysts. *Topics in Catalysis*, **8** (1999) 57–63

25. S. Nie and S.R. Emory, Science 275, 21, 1102 (1997).